Indian Journal of Pure & Applied Physics
Vol. 60, September 2022, pp. 754-762
DOI: 10.56042/ijpap.v60i9.60690

Power Quality Improvement of a Fuel Cell-Powered Filterless Distributed Generation System Using Sinusoidal Pulse Width Modulation

Shubham Kumar Singh, Anshul Agarwal* & Tirupathiraju Kanumuri
National Institute of Technology, Delhi, 110 040, India

Received 20 February 2022; accepted 19 April 2022

This paper proposes a distributed generation system based on fuel cells and batteries. The primary energy source for the distributed generation system is a proton exchange membrane fuel cell, with a lead-acid battery serving as the energy storage medium. A boost converter regulates the output power of a fuel cell to guarantee smooth operation. The battery is connected with the fuel cell to meet the power demand of the distributed generation system. A buck-boost bidirectional converter is employed as an interface between the battery and the DC link capacitor. The bidirectional converter operates on the slope compensated current control approach. Two 5-level cascaded H-bridge inverters have been installed to improve the power quality of distributed generation systems. The power flow between the source, grid, and nonlinear load is controlled using a sinusoidal pulse width modulation approach. Nonlinear current compensation and capacitor voltage balancing are two features that improve power quality.

Keywords: Fuel cell; Lead-acid battery; Bi-directional converter; Shunt Active Power Filter (SAPF); Non-linear load

1 Introduction

Traditional fossil fuels such as coal, natural gas, and petroleum have been primary energy sources. The extensive usage of these fossil fuels is a significant source of pollution[1]. Due to significant environmental challenges, all humanity must adopt renewable energy sources[2,3]. Furthermore, rising electricity consumption creates substantial challenges for power system operators, such as transmission losses[4,5]. In the electricity business, distribution generating systems (DGs) are among the most well-known remedies for transmission losses. Grid-connected and islanded operations have several advantages, including improved power quality and reliability, more flexible power generation, and higher penetration of distributed generation (DG)[6]. Renewable energy sources must be used as a primary source for DG in the future energy market. Hydrogen energy is a long-term, environmentally friendly energy source employed in a distributed generation system.

In recent years, Fuel cells (FC) have become widely recognised as an essential component of micro grids[7]. The speed of the chemical reaction determines the responsiveness of the fuel cell. Alkaline fuel cells (AFCs), proton exchange membrane fuel cells (PEMFCs), solid oxide fuel cells (SOFCs), phosphoric acid fuel cells (PACs), molten carbonate fuel cells (MCFCs), and microbial fuel cells are examples offuel cells. The proton exchange membrane fuel cell (PEMFC) is a widely used electrochemical energy conversion technique that converts hydrogen into electricity directly[8]. PEMFCs have several benefits: high power density, quiet operation, a low operating temperature that allows for a quick start-up time, negligible electrolyte leakage due to the solid polymer membrane, and no pollution emissions[9]. As a result, PEMFC has found applications in various industries, including transportation and power generation[10,11].

There are several issues with FCs, including their low durability and expensive pricing[12]. In addition, challenges such as system control, hybridisation, energy management, and the reliability of micro-grids must be addressed[13].Unfortunately, PEMFC produces low dc voltage; As a result, in the fuel cell power generating system, a DC-DC converter is necessary to increase the low dc voltage to a higher voltage[14]. PEMFCs are good competitors for generating stable energy, but they have poor transient performance for power loads[15], affecting the system's stability, reliability, and robustness. As a result, to fulfil the micro-grid goal, PEMFCs are routinely paired with other energy storage devices[16,17]. For usage of energy storage devices in DG systems, lead-acid batteries are suitable, low-cost, and widely available. So, a DG system with fuel cells and batteries could be an

*Corresponding author: (E-mail: anshul@nitdelhi.ac.in)

effective nonlinear load operation combination. The DG system also requires good energy management to attain high efficiency, low fuel costs, long battery life and FC life[18]. Nonlinear loads, such as uninterruptible power supplies (UPS) and energy-efficient lighting require nonlinear current from the source due to harmonics. The non-sinusoidal current distorts the voltage at the point of common coupling (PCC)[19]. Other loads connected to PCC are affected by the distorted voltage. As a result, filters and compensators are necessary to solve these issues. To adjust for nonlinear current drawn by harmonic generating (nonlinear) loads, active power filters (APF) are often used. Nonlinear load draws current having harmonic components, typically rectified using shunt active power filters. A DG system with a filter is more complicated and expensive. Even using capacitors and inductors with a short operating life raises the system's maintenance costs.

So, the objective of the paper is:

- A design for a household FC-battery-powered distributed grid system with enhanced power quality.
- Elimination of filter which makes system bulkier and costly

2 Fuel cell-battery powered DG system with enhanced power quality feature.

A schematic diagram of a fuel cell (PEMFC) and lead-acid battery-powered DG system has been illustrated in Fig. 1 to address the power quality issue.

The suggested system includes a DC-DC converter, an inverter, a non-linear load, a primary fuel cell (PEMFC), and a lead-acid battery. The fuel cell was operated at the desired level using a DC-DC boost converter[20].A buck-boost bidirectional converter was employed to connect a lead-acid battery to a fuel cell. Two 5-level cascaded H-Bridge multi-level inverters were used to accomplish the power quality improvement function, which includes DC link voltage stability and harmonics compensation created by the load. For the non-linear load, a single-phase uncontrolled rectifier with RL load was used.

2.1 Proton Exchange Membrane Fuel Cell System

The suggested system includes a DC-DC converter, an inverter, a non-linear load, a primary fuel cell (PEMFC), and a lead-acid battery. The fuel cell was operated at the desired level using a DC-DC boost converter[20]. A buck-boost bidirectional converter was employed to connect a lead-acid battery to a fuel cell. Two 5-level cascaded H-Bridge multi-level inverters were used to accomplish the power quality improvement function, which includes DC link voltage stability and harmonics compensation created by the load. For the non-linear load, a single-phase uncontrolled rectifier with RL load was used. A typical schematic representation of a PEMFC has been shown in Fig. 2. To calculate the system output voltage, vapour and water pressures are taken into account in the semi-empirical model[20]. The internal resistance of the PEMFC, particularly the electronic and ionic

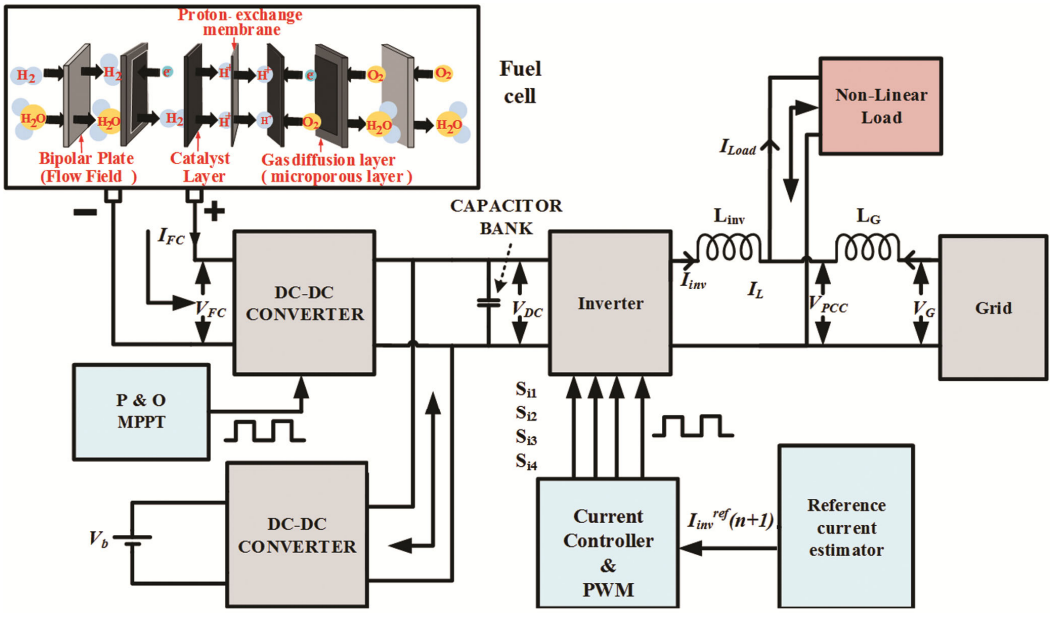

Fig. 1 — Schematic diagram of fuel cell-battery powered DG systemwith enhanced PQ features.

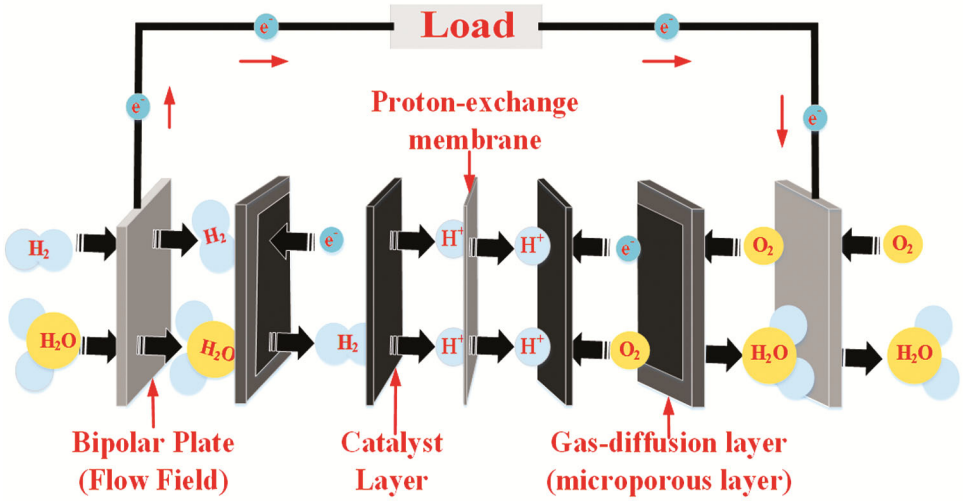

Fig. 2 — The schematic diagram for the PEMFC fuel cell.

resistances, is a significant factor determined by the temperature, water content, and loading circumstances. Due to non-linear voltage losses in the system, calculating the voltage of an FC is difficult. Activation and concentration voltage drops are non-linear, but an ohmic voltage drop is linear. An equivalent electrical model of fuel cell has been shown in Fig. 3.

The total output voltage of a PEMFC system is given as:

$$V_{out} = V_{nl} - V_{act} - V_{ohmic} - V_{con} \quad ...(1)$$

V_{nl} represents the no-load voltage, V_{act} represents the activation voltage drop, V_{ohmic} represents the ohmic voltage drop, and V_{con} represents the system's concentration voltage drop. The Nernst equation has been used to calculate the potential[20]. E_{cell} of a PEMFC system is obtained by the following equation:

$$E_{cell} = E_{0,cell} + \frac{RT}{2F} ln\left(\frac{P_{H2} P_{O2}^{0.5}}{P_{H2O}}\right) \quad ...(2)$$

The partial hydrogen, oxygen, and water pressures are represented as P_{H2}, P_{O2}, and P_{H2O}, respectively.

$$E_{0,cell} = 1.229 - 8.5 \times 10^{-4} (T - 298) \quad ...(3)$$

Since a stack of PEMFC is the combination of n cells connected in series, the total EMF produced by stack E_{stack} is given as:

$$E_{stack} = nE_{cell} \quad ...(4)$$

The no-load voltage V_{nl} is less than the EMF of the cells because of internal currents flowing through the circuit and a voltage drop produced[20].

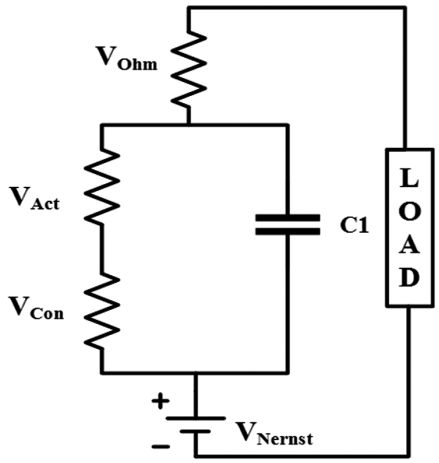

Fig. 3 — Equivalent circuit electrical model of the fuel cell.

$$n(V_{int} + V_{H2O}) = A_1 T P_{H2} + A_2 \quad ...(5)$$

$$V_{no,load} = n\left[E_{0,cell} + \frac{RT}{2F} ln(P_{H2} P_{O2}^{0.5}) - (V_{int} + V_{H2O})\right] \quad ...(6)$$

Where V_{int} is the voltage drop due to internal currents; V_{H2O} is the voltage drop due to the pressure of water P_{H2O}, and V_{int}+V_{H2O} is extracted using temperature T and P_{H2}. Where A_1 and A_2 are empirical expression constants and are given as 0.0219 and 18.8223, respectively[20]. T and P_{H2} are taken from the internal sensors of the PEMFC system[20]. In most commercial PEMFC systems, the applied pressure of hydrogen fuel is known. The following equation expresses the activated voltage drop:

$$V_{act} = \frac{RT}{2\alpha F} ln\left(\frac{I}{i_O}\right) \quad I > i_O \quad ...(7)$$

Where I is current, α is the charge transfer coefficient, and i_o is the current exchange density given as:

$$i_O = B_1 F \exp\left(\frac{-1.229 B_2 F}{RT}\right) \quad ...(8)$$

Where B_1 and B_2 are the coefficients. The ohmic voltage drop is given as:

$$V_{ohm} = I\left(R_{ionic} + R_e\right) \quad ...(9)$$

Where R_{ionic} is the ionic resistance; and R_e is the electronic resistance. To calculate R_{ionic}, the relative humidity ϕ and membrane water content λ_m must be obtained.

$$\phi = \frac{P_{H2O}}{P_{vap}} \quad ...(10)$$

Where P_{vap} is the vapour pressure of the PEMFC system.P_{H2O} is extracted by (6) using V_{H2O}, and V_{int} is 0.09. The equations for calculating P_{H2O} are as follows:

$$P_{H2O} = exp\left(\frac{V_{H2O}}{TA_{H2O}}\right) \quad ...(11)$$

Where A_{H2O} is the empirical expression constant for the pressure of water. After calculating the relative humidity, the membrane water content λ_m, which is the polynomial expression of relative humidity, is presented as:

$$\lambda_m = 0.043 + 17.81\phi - 39.85\phi^2 + 36\phi^3 \quad ...(12)$$

The primary purpose for calculating membrane water content λ_m is to calculate R_{ionic}, which is dependent on the current, temperature, and membrane water content of PEMFC:

$$R_{ionic} = \frac{C_1\left[1 + 0.03I + 0.062\left(\frac{T}{303}\right)^2 I^{2.5}\right]}{\left(\lambda_m - 0.634 - 3I\right)\exp\left(4.18\left(\frac{T-303}{T}\right)\right)} \quad (13)$$

...

Where C_1 is a constant related to the membrane thickness. R_e is taken as constant for simplicity. However, it is determined by the membrane's electronic conductivity and thickness in reality. The change in concentration voltage drop depends on the loading current. The concentration voltage V_{con} is obtained from[20] as:

$$V_{con} = \frac{-NRT}{2F} ln\left(1 - \frac{I}{I_{lim}}\right) \quad ...(14)$$

Where N is the population size; and I_{lim} is the maximum current limit from the PEMFC system.

2.2 Modified Semi-Empirical Model

The main limitation in the model mentioned above is the use of sensors to obtain the partial pressure of hydrogen and the assumption that the pressure of oxygen is atmospheric. The partial pressure of hydrogen is not measurable in most commercial PEMFC systems. Furthermore, the partial pressure of oxygen within a PEMFC system differs from the ambient pressure. The temperature of the PEMFC system affects the vapour pressure inside the system. The fluctuation in partial pressures of oxygen and hydrogen is caused by such vapour pressure. The equation for partial pressures of oxygen and hydrogen is used in this study[21]. The formula is taken for determining the pressure of oxygen P_{O2} from the given data[21]. The expression for calculating the pressure of oxygen P_{O2} from the input pressure at the cathode P_{ca}, which is the atmospheric pressure of air[21], is expressed as:

$$P_{O2} = \frac{P_{ca} - 0.5P_{vap}}{4.76} \quad ...(15)$$

The constant factor of 0.5 is attributed to the relative humidity of the air, which ranges between 40% and 50%, whereas 4.76 is a universal constant. The expression for determining hydrogen pressure is also dependent on the PEMFC system's P_{vap} and the hydrogen inlet pressure P_{an}. The constant C_2 is used in the equation to account for the cathode and anode's typical relative humidity.

$$P_{H2} = P_{an} - C_2 P_{vap} \quad ...(16)$$

Considering these realistic approaches in calculating P_{O2} and P_{H2}, the calculation of no-load voltage will be different. Thus, A_1 and A_2 in (6) must be optimised. However, in reality, the electronic resistance is dependent on PEMFC temperature. A new modified expression for electronic resistance can be expressed as:

$$R_e = \frac{D_1}{T} + D_2 \quad ...(17)$$

The total ohmic resistance R_{ohmic} will be given by:

$$R_{ohmic}=\frac{C_1\left[1+0.03I+0.062\left(\frac{T}{303}\right)^2 I^{2.5}\right]}{(\lambda_m-0.634-3I)\exp\left(4.18\left(\frac{T-303}{T}\right)\right)}+\frac{D_1}{T}+D_2 \quad ...(18)$$

The constants D_1 and D_2 should be optimised. Note that R_e only depends on PEMFC temperature.

3 MPPT for PEMFC

In a PEMFC power system, the MPPT control method is essential to obtain high efficiency. According to the PEMFC's mathematical modelling, changes in load or fuel cell parameters can substantially impact the fuel cell's output power. Changes in the operational temperature of the fuel cell will cause the MPP of the fuel cell to vary. Fig. 4 (a & b) depicts the P-I and V-I curve of PEMFC respectively. For PEMFC, MPPT methods such as P&O can track the MPP. The PEMFC parameters are used in the MPPT algorithm to determine the optimal switching state for the DC-DC boost converter.

4 Mathematical modelling of system

Various parameters of the system can be expressed using the following equations.

$$V_{inv}=\sum_{i=1}^{2} V_{DCi}\left(S_{i1}-S_{i2}\right) \quad ...(19)$$

Here S_{i1}=S_{i4} and S_{i2}=S_{i3}, whereS_{i1}, S_{i2}, S_{i3}, S_{i4} are gate pulse for i^{th} H-bridge inverter.

$$V_{inv}=L_{inv}\frac{dI_{inv}}{dt}+V_P \quad ...(20)$$

$$V_G=L_G\frac{dI_G}{dt}+V_P \quad ...(21)$$

$$V_P=L\frac{dI_L}{dt}+RI_L-2V_D \quad ...(22)$$

Here L_{inv}, L_G, V_P, V_D are inverter side inductance, grid side inductance, the voltage at the PCC and the voltage drop across the diode, respectively.

4.1 Control Scheme of Proposed fuel cell-powered distributed generation system (PQEC feature)

A fuel cell DG system having enhanced power quality features is depicted in Fig. 1. A DC-DC converter has been used to obtain the fuel cell module's required output. An inverter has been used to convert DC electricity into AC electricity. The inverter was controlled using the SPWM technique. Grid current I_g, load current I_L, inverter current I_{inv}, active and reactive power have been studied, and power quality enhancement features have been coupled with the inverter. The load current is obtained from the inverter and grid in load sharing situations and calculated using the formula below.

$$I_L=I_{inv}+I_G \quad ...(23)$$

4.2 Inverter power flow control

DC-link voltage is matched to a set reference voltage (V_{DC}*). The reference current is obtained using the following equations to generate gate pulse using the SPWM technique.

$$\Delta V(n)=V_{DC}^{*}(n)-V_{DC}(n) \quad ...(24)$$

$$I_1(n)=I_1(n-1)+K_p[\Delta V(n)-\Delta V(n-1)]+K_I\Delta V(n) \quad ...(25)$$

Here $I_1(n)$ is the output of the PI controller at the n^{th} instance, whereas the constants K_P and K_I are proportional and integral constants of the PI controller for the DC link voltage balancing block.

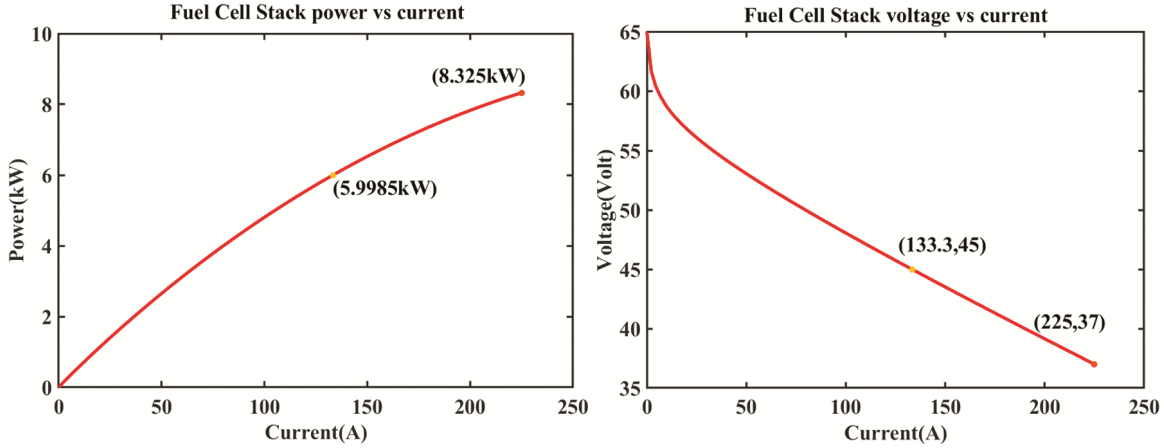

Fig. 4 — (a) PEMFC P-I curve. (b) PEMFC V-I curve.

So the output I_1 of the controller is given as

$$I_1(n)=I_1(n-1)+K_{p1}[\Delta V_1(n)-\Delta V_1(n-1)]+K_{I2}\Delta V_1(n) \quad \text{...(26)}$$

As a result, the output of the DC-link voltage control loop I_v is as follows:

$$I_V(n)=I_1*V_{gu}(n) \quad \text{...(27)}$$

Where V_{gu} (n) is the unit template of grid voltage at n^{th} instant. After that, the load current is added to the equation to provide reference current based on the load requirement.

$$i_{inv}^{ref}=I_V(n)+I_L(n) \quad \text{...(28)}$$

This causes the inverter current to track the load current at the previous instant.

5 Results

A fuel cell battery-based DG system is simulated to achieve harmonic current compensation, power factor correction, and active and reactive power flow regulation. Two fuel cell stacks and two batteries have been used as sources of two 5-level H bridge cascaded inverters. A control strategy has been developed to evaluate the effectiveness of integrating lead-acid batteries with fuel cells and PQEC features for the non-linear load. Fig. 5 depicts the output of DC-link capacitor voltage. As shown in Fig. 5 the fluctuation in the DC-link voltage occurs due to an imbalance of the input and output power. So to maintain the DC-link voltage, there must be a balance of power across the DC-link capacitor. Hence, the boost converter and the bi-directional converter has been implemented to maintain the DC link capacitor voltage. The bi-directional converter has been operated in buck and boost mode depending on battery charging and discharging. FC has been used at the maximum power point to get maximum power. The battery is disconnected when its SOC is out of the upper and lower threshold limit. In Fig. 5, initially, PQEC was kept off till 0.1 seconds. PQEC is turned on from 0.1 seconds onwards. Fluctuation occurred in DC-link capacitor voltage due to transient as shown in Fig. 5.

The SPWM control approach was used to operate 5-level cascaded H-bridge multilevel inverters. The grid voltage, load current, and DC-link voltage are used to calculate the reference compensating current. Two 5-level cascaded H-bridge inverter supplies nonlinear current. An uncontrolled rectifier with R=10Ω, L=10mH and R=20Ω, L=25mH on the DC side is used as non-linear loads for the inverter's local load. The load current, grid current, and inverter current are shown in Fig. 6 Under various loading conditions, the performance was evaluated for THD improvement and reactive power compensation and displayed in Fig. 6-10. The nonlinear load current is divided into the linear and harmonic components. The grid provides the linear component of load requirement, while the harmonics are compensated by the fuel cell-battery powered inverter.

The operation of the model contains two modes.

Mode 1

In this mode, the PQEC feature is turned off. In Fig. 6 first mode is simulated from t = 0 to t = 0.1 sec. So, the inverter does not supply any harmonic component required by the load. It feeds the load by

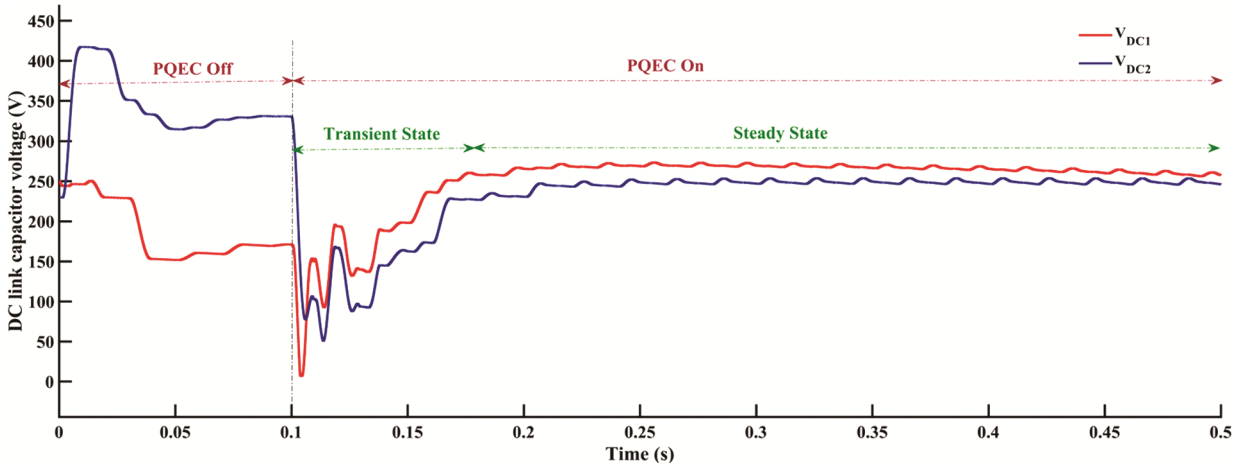

Fig. 5 — Outputwaveforms ofDC-link voltagefor two 5-level cascaded MLI as shunt active power filters for the grid-connected fuel cell-battery based system with the non-linear load.

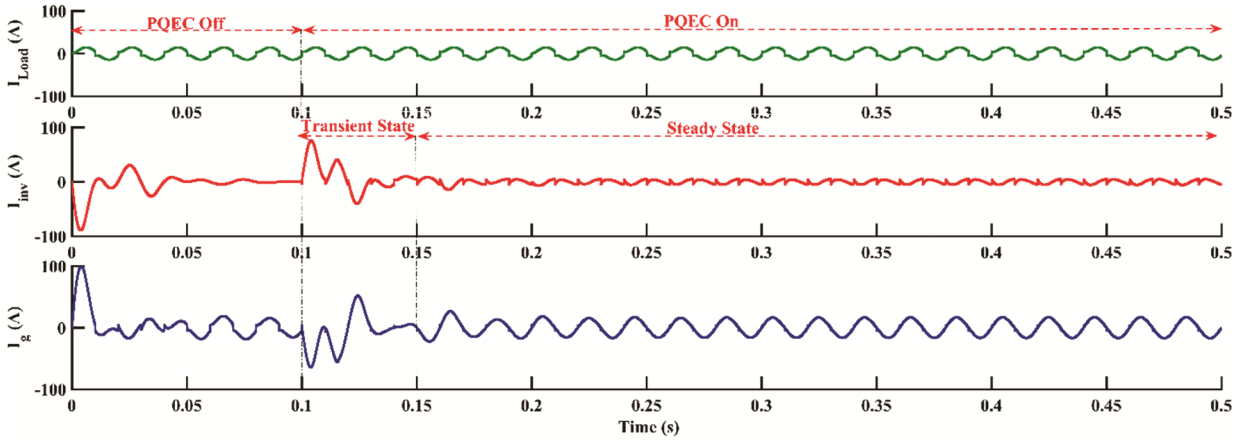

Fig. 6 — Output waveforms of the load, inverter, and grid current for a different mode of operation for a non-linear load having R=20 Ω, L=25mH.

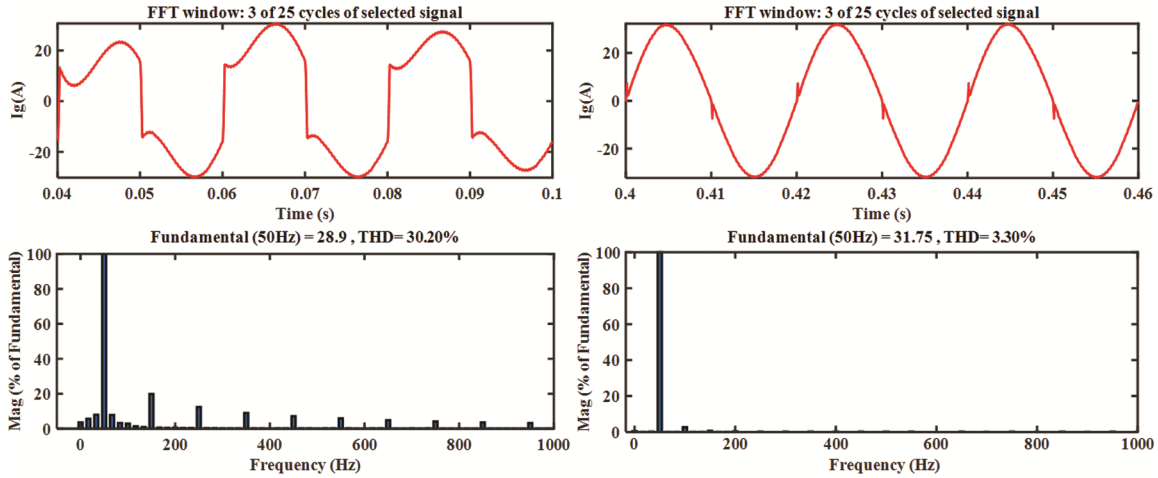

Fig. 7 — (a) Spectrum of grid current during mode 1 (when PQEC is off) and (b) Spectrum of grid current during mode 2 (when PQEC is on) for non-linear load having R=10 Ω, L=10mH.

converting available DC power to AC power. The grid provides the linear as well as harmonic content of the load.

Mode 2

In this mode, the power quality enhanced feature is turned on. In Fig. 6, mode two is started from t=0.1 sec onwards. The inverter supplies a non-linear load current component (required by the load). The grid provides the remaining linear component needed for the load. As depicted in Fig. 6, the system shows transient behaviour for 0.1 sec to 0.15 sec. From 0.15 sec onwards system provides the steady-state output.

During mode 1 grid supplies the current to the non-linear load having R=10 Ω, L=10 mH. Fig. 7 (a) shows the grid current with the harmonic spectrum for mode 1 when the PQEC feature is off. In mode 1 grid has to supply 28.9A with THD of 30.2%. Fig. 7 (b) shows the grid current and the harmonic spectrum for mode 2 when the PQEC feature is turned on. In this mode grid supplies the linear component of the current demanded by the non-linear load. The inverter compensates for the load's non-linear current and reactive power demands. The grid must provide only the active and linear components of the load demand. I_L has a THD requirement of 30.2% of its fundamental component, out of which I_g supplies 31.75A with 3.30% THD, and I_{inv} provides the remaining nonlinear component of load current. Fig. 8 (a) depicts the harmonics of grid voltage at PCC during mode 1 for the non-linear load. In the mode 1 grid voltage at PCC has THD of 1.67%.Fig. 8 (b) depicts the harmonics of grid voltage at PCC with THD of 1.21% for the non-linear load.

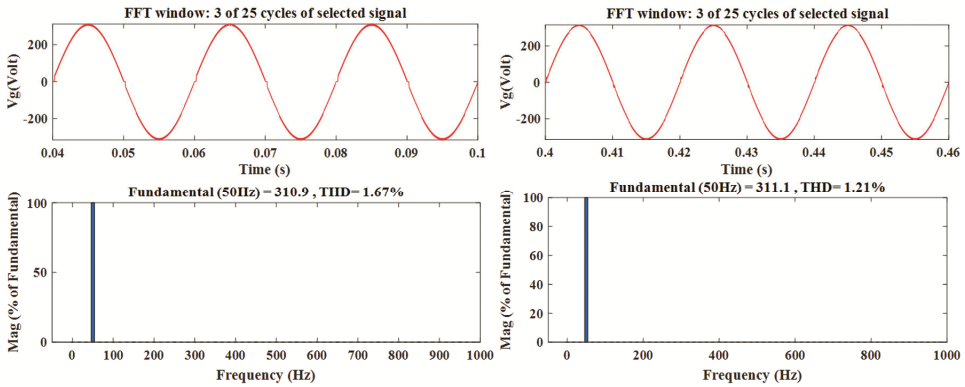

Fig. 8 — (a) Spectrum of PCC voltage during mode 1 (when PQEC is off) and (b) Spectrum of PCC voltage during mode 2 (when PQEC is on) for non-linear load having R=10 Ω, L=10mH.

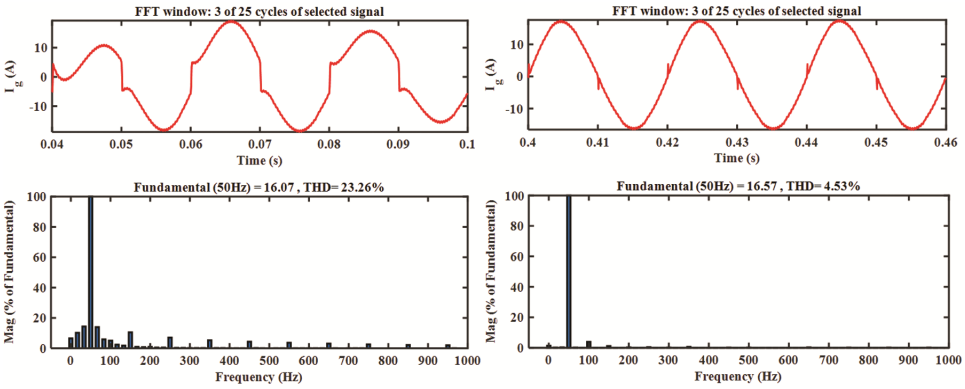

Fig. 9 — (a) Spectrum of grid current during mode 1 (when PQEC is off) and (b) Spectrum of grid current during mode 2 (when PQEC is on) for non-linear load having R=20 Ω, L=25 mH.

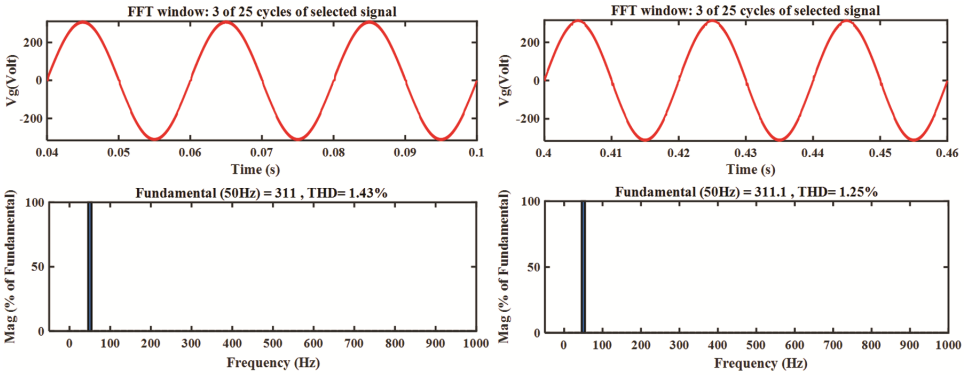

Fig. 10 — (a) Spectrum of PCC voltage during mode 1 (when PQEC is off) and (b) Spectrum of PCC voltage during mode 2 (when PQEC is on) for non-linear load having R=20 Ω, L=25mH.

Whereas Fig. 9 (a) shows the grid current and harmonic spectrum for mode 1having non-linear load having R=20 Ω, L=25mH. In mode 1the PQEC feature is off and grid has to supply current with THD of 23.26%. Fig. 9 (b) shows the grid current and the harmonic spectrum for mode 2 when the PQEC feature is turned on. In this mode the inverter compensates for the load's non-linear current and reactive power demands. The grid has to supply the linear component of the current demanded by the non-linear load. Fig. 9 (b) demonstrate that the grid supplies 16.57A current with 4.53 percent THD and the inverter delivers the remaining nonlinear component of load current to meet the load's THD requirement. Fig. 10 (a) depicts the harmonics of grid voltage at PCC for the non-linear load having R=20

Ω, L=25mH. In the mode 1 grid voltage at PCC has a THD of 1.43%. Fig. 10 (b) depicts the harmonics of grid voltage at PCC during mode 2 (when PQEC is on).In mode 2, THD of grid voltage at PCC is 1.25% for the non-linear load.

6 Conclusions

In this Paper fuel cells and batteries are used as a source for the proposed system. Modelling and controlling the fuel cell and the lead-acid battery has been done. Fuel cell-battery based DG system has been designed and simulated with improved power quality features. SPWM technique has been implemented to operate the inverter and eliminate the harmonics generated by load without a filter. The simulation base studies can decrease THD for the non-linear load. For the load having R=10 Ω and L=10mH, THD of grid current decreases from 30.2% to 3.3%. With the load having R=20 Ω and L=25mH, THD of grid current drops from 23.26 % to 4.53%. DC-link capacitor voltage balancing is also being achieved. It is observed that the proposed system eliminated the need for a filter for the load, and the cost of the system is also being reduced.

References

1 Soumeur M A, Gasbaoui B, Abdelkhalek O, Ghouili J, Toumi T & Chakar A, *J Power Sources*, 462 (2020) 228167.

2 Singh S K, Agarwal A & Kanumuri T, *J Eng Res* (*JER*), *Kuwait* (*in press*).

3 Kumar N & Agarwal A, *Indian J Pure Appl Phys*, 59 (2021) 206.

4 Tatabhatla V M R, Agarwal A, Kanumuri T, *IEEE Trans Power Electron,* 36 (2021) 4214.

5 Panigrahi R, Mishra S K & Srivastava S C, *A Rev IEEE Trans Ind Appl,* (2020).

6 Shah S A A, *Int J Hydrogen Energy*, 45 (2020) 15841.

7 Elsaid K, Sayed E T, Abdelkareem M A, Baroutaji A & Olabi Y A, *Sci The Total Environ*, 740 (2020) 140125.

8 Hu J, Zhu J & Dorrell D G, *IET Renewable Power Generation*, 8 (2014) 240.

9 Hu J, Li Z, Zhu J, & Guerrero J M, *IEEE Indus Electron Mag*, 13 (2019) 17.

10 Li Q, Su B, Pu Y, Han Y, Wang T, Yin L & Chen W, *IEEE Trans Transport Electrificat*, 5 (2019) 552.

11 Zhou D, Gao F, Breaz E, Ravey A, Miraoui A & Zhang K, *IEEE Trans Energy Conversion*, 31 (2016) 1399.

12 Chen J, Liu Z, Wang F, Ouyang Q & Su H, *IEEE Trans Control Syst Technol*, 26 (2017) 1711.

13 Das V, Padmanaban S, Venkitusamy K, Selvamuthukumaran R, Blaabjerg F & Siano P, *Renewable Sustainable Energy Rev*, 73 (2017) 10.

14 Yoldaş Y, Onen A, Muyeen S M, Vasilakos A V & Alan I, *Renew Sustain Energy Rev*, 72 (2017) 205.

15 He H, Quan S & Wang Y X, *Int J Hydrogen Energy*, 45 (2020) 20382.

16 Li Q, Su B, Pu Y, Han Y, Wang T, Yin L & Chen W, *IEEE Trans Transport Electrificat*, 5 (2019) 552.

17 He H, Quan S, Sun F & Wang Y X, *IEEE Tran Indus Electron*, 67 (2020) 9012.

18 Sulaiman N, Hannan M A, Mohamed A, Ker P J, Majlan E H & Daud W, *Appl Energy*, 228 (2018) 2061.

19 Ma C, Dasenbrock J, Tobermann J C & Braun M, *Appl Energy*, 242 (2019) 674.

20 Khan S S, Shareef H, Wahyudie A & Khalid S N, *Int J Energy Res*, 42 (2018) 2615.

21 Zhang J, Tang Y, Song C, Xia Z, Li H, Wang H & Zhang J, *Electrochimica Acta*, 53 (2008) 5315.